Carbohydrate Polymers 266 (2021) 118105

Contents lists available at ScienceDirect

Carbohydrate Polymers

journal homepage: www.elsevier.com/locate/carbpol

Polyvinyl alcohol as a crucial omissible polymer to fabricate an impedimetric glucose biosensor based on hierarchical 3D-NPZnO/chitosan

Sahere Khazaei, Sayed Ahmad Mozaffari *, Fateme Ebrahimi

Thin Layer and Nanotechnology Laboratory, Department of Chemical Technology, Iranian Research Organization for Science and Technology (IROST), P.O. Box 33535-111, Tehran, Iran

ARTICLE INFO

Keywords:
Chitosan
Polyvinyl alcohol
Glucose biosensor
3D-ZnO nanostructure
Impedimetric biosensing

ABSTRACT

Highly stable and reliable monitoring of glucose is of great importance for diabetes patients. This paper describes the application of two types of polymer for developing a reliable impedimetric glucose biosensor by designing an efficient nanoporous microenvironment for enzyme loading. Polyvinyl alcohol (PVA) was used as a sacrifice polymer to prepare a uniform 3D-nanoporous ZnO (3D-NPZnO) platform through electrodeposition of ZnO/PVA layer followed by PVA elimination via annealing. The carbohydrate polymer, chitosan (CTS), with a high isoelectric point (pI = 7.0–9.0), was selected in accompanying with 3D-NPZnO (pI = 9.5) to provide a hierarchical 3D-NPZnO/CTS microenvironment of a favorable isoelectric point for glucose oxidase enzyme (pI = 4.2) loading. The characterization of structural features and monitoring of the biosensor fabrication process was performed using FE-SEM, EDX, TGA-DTG, FTIR, UV–Vis, BET-BJH, XRD, CV, and EIS techniques. The fabricated platform, which shows a wide linear range of 1.0–18.0 mM and a low detection limit of 0.2 mM for glucose determination, was successfully used for real sample analysis. The proposed fabrication method can be applied for immobilizing the other low isoelectric point enzymes and biomolecules.

1. Introduction

Enzyme-involved electrochemical glucose biosensors were extensively studied due to the increasing demand of diabetic patients as well as medical diagnostic laboratories for accurate and reliable monitoring of serum glucose levels (Asrami et al., 2020; Ocvirk et al., 2016). In this regard, polymer-assisted synthesis methods have received substantial attention for constructing biosensing transducers with high enzyme loading capacities as an important bottleneck in the development of novel biosensors (Dakshayini et al., 2019; El-Naggar & Shoueir, 2020; Fadillah et al., 2020; Li et al., 2019; Rahmanian et al., 2015). Concurrently, many different nanostructures of metal oxides have been designed to meet the needs of biosensing platforms owing to their special property for promoting kinetics of electron transfer between the active sites of enzyme and the electrode surface (Asrami et al., 2017; Asrami et al., 2018; Kucherenko et al., 2019). One interesting strategy for increasing the enzyme loading capacities of transducer of a biosensor is the use of sacrificing polymers as organic additives in synthesis of metal oxide nanoparticles. These polymers could participate in the fabrication process by forming a polymer-metal oxide hybrid film. Then, after being sacrificed via thermal omission, the polymers leave a three-dimensional and porous structure of the desired metal oxide with capability of maintaining a high enzyme load in its nanoporous structure (Kumar et al., 2018; Mallakpour & Madani, 2015; Sarkar et al., 2012). On this basis, PVA is a biocompatible polymer with characteristics such as water solubility, and the capability of decomposition in rather low temperatures (Schué, 2000). This makes PVA a suitable sacrifice polymer for use in the polymer-assisted electrochemical synthesis of metal

Abbreviations: DAP, poly (2,6-diaminopyridine); Au NPs, Au nanoparticles; BSA, bovine serum albumin; CHIT/CAR, chitosan/κ carrageenan; CLNS, complex nonlinear least-squares method; CTS, chitosan; CV, cyclic voltammetry; DTG, differential thermal analysis; EDX, energy dispersive spectroscopy; EIS, electrochemical impedance spectroscopy; FE-SEM, field emission scanning electron microscopy; FTIR, Fourier transform infrared spectroscopy; FTO, fluorine doped tin oxide; GLM, glucose oxidase liposome microreactor; GOx, glucose oxidase; GR, graphite rod; ITO, indium tin oxide; MPC, mesoporous carbon; MWCNT, multi-wall carbon nanotube; 3D-NPZnO, 3-dimensional nanoporous zinc oxide; PEC, polyelectrolyte complex; p*I*, isoelectric point pH; PMMA, poly(methylmethacrylate); PPY, polypyrrole; PVA, polyvinyl alcohol; RGO, reduced graphene oxide; TGA, thermogravimetric analysis; UV–Vis, ultraviolet-visible spectroscopy; ZnO, zinc oxide; ZnO NRs, zinc oxide nanorods.

* Corresponding author.
E-mail address: mozaffari@irost.ir (S.A. Mozaffari).

https://doi.org/10.1016/j.carbpol.2021.118105
Received 16 September 2020; Received in revised form 4 March 2021; Accepted 21 April 2021
Available online 24 April 2021

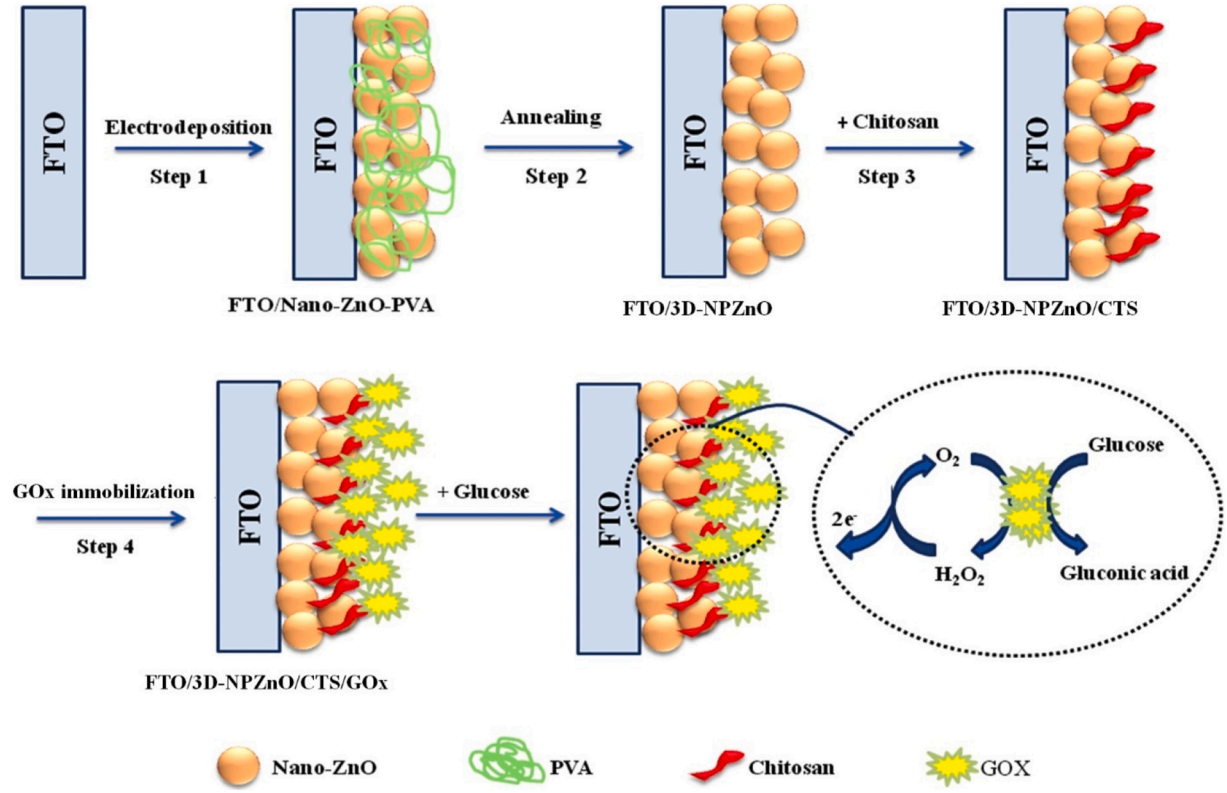

Fig. 1. The schematic illustration of FTO/3D-NPZnO/CTS/GOx biosensor fabrication and the mechanism of biosensor's response to glucose.

oxide nanostructures (Mozaffari et al., 2014; Pauporté, 2007). ZnO is one of the promising metal oxides due to its important properties such as non-toxicity, chemical stability, electrical conductivity and biocompatibility. Because of these favorable properties, ZnO has received great attention in the field of fabricating various nanostructures for different applications such as solar cells (Kouhestanian et al., 2020), and sensing platforms (Moharamzadeh et al., 2018; Mozaffari et al., 2015).

In addition to the construction of transducer surface, enzyme immobilization strategy emerges as a fundamental aspect for developing efficacious biosensors with suitable analytical performances (Sassolas et al., 2012; Wahab et al., 2020). Recently, polymers have been used to fabricate biosensors (Dong et al., 2021; Gupta et al., 2020). Chitosan (CTS) is a naturally derived polymer representing one of the most technologically important classes of active materials with application in various industrial and biomedical fields. It is one of the interesting biopolymers in sensor fabrication, especially in terms of enzyme immobilization, because of its abundant functional groups, high permeability, good mechanical strength, non-toxicity, and low cost (Dutta et al., 2004).

Compared to the other valuable electrochemical methods applied in the glucose-sensing area, such as potentiometric (Cánovas et al., 2020; Zhang et al., 2020), amperometric (Kausaite-Minkstimiene et al., 2020), and conductometric (Kucherenko et al., 2016) techniques, the role of electrochemical impedance spectroscopy (EIS) as an authoritative technique for strongly advantageous non-destructive measurements has been less considered. Several advantageous have been offered for EIS technique over other electrochemical methods. These advantageous include the fact that it is a steady-state technique, employs small signal amplitude, and that is capable of investigating interfacial reaction mechanisms over a very wide frequency range (<1 mHz to >1 MHZ) using readily available instrumentation. EIS is a well-known electrochemically nondestructive evaluation method which does not damage or disturb bio-recognition layer. However, the EIS accuracy depends on different sources: measurements and model, and requires fitting a model to perform complex computations (Pastor-Fernández et al., 2017). In addition, the interpretation of impedance data needs more skills and expertise than other electrochemical methods (Macdonald, 1990). EIS can provide information on electrode/electrolyte interface characteristics, which belong to the recognition events at the modified electrode surface (Duran et al., 2019; Mozaffari et al., 2015; Shabani et al., 2009).

In this research, unique properties of chitosan biopolymer (isoelectric point of about 7.0–9.0) in association with 3D nanoporous ZnO (3D-NPZnO, the isoelectric point of 9.5) were used as a key strategy to significantly improve biosensing behavior through the provision of some criteria, including (i) exploiting highly porous ZnO as an efficient charge transducer with proper interaction with chitosan layer, (ii) using chitosan with abundant hydroxyl and amine groups as an excellent platform area for electrostatic immobilization of glucose oxidase enzyme (GOx), (iii) improving enzyme loading by using dissimilarity between isoelectric points of 3D-NPZnO-CTS (p$I \approx 9.0$) platform and GOx enzyme (p$I = 4.2$) as a driving force to achieve highly stable enzyme loading. Also, appealing features of the EIS technique were employed to develop a reliable electrochemical glucose biosensor. Accordingly, this approach resulted in the successful application of the fabricated biosensor for glucose determination in a biological sample with high sensitivity and reproducibility.

2. Experimental

2.1. Materials and apparatus

D(+)-glucose anhydrous for biochemistry (Merck), Glucose oxidase (G6766–10,000 units/g solid from Aspergillus niger, without added oxygen, Sigma Aldrich), Polyvinyl alcohol (PVA, 85–124 kDa, 87–89% hydrolyzed, Alfa Aesar), chitosan (Sigma-Aldrich) with the average molecular weight of 150 kDa (determined by gel permeation chromatography), and deacetylation degree of 83% (determined by ^{1}HNMR), zinc chloride ($ZnCl_2$, Merck), potassium chloride (KCl, Merck) used as

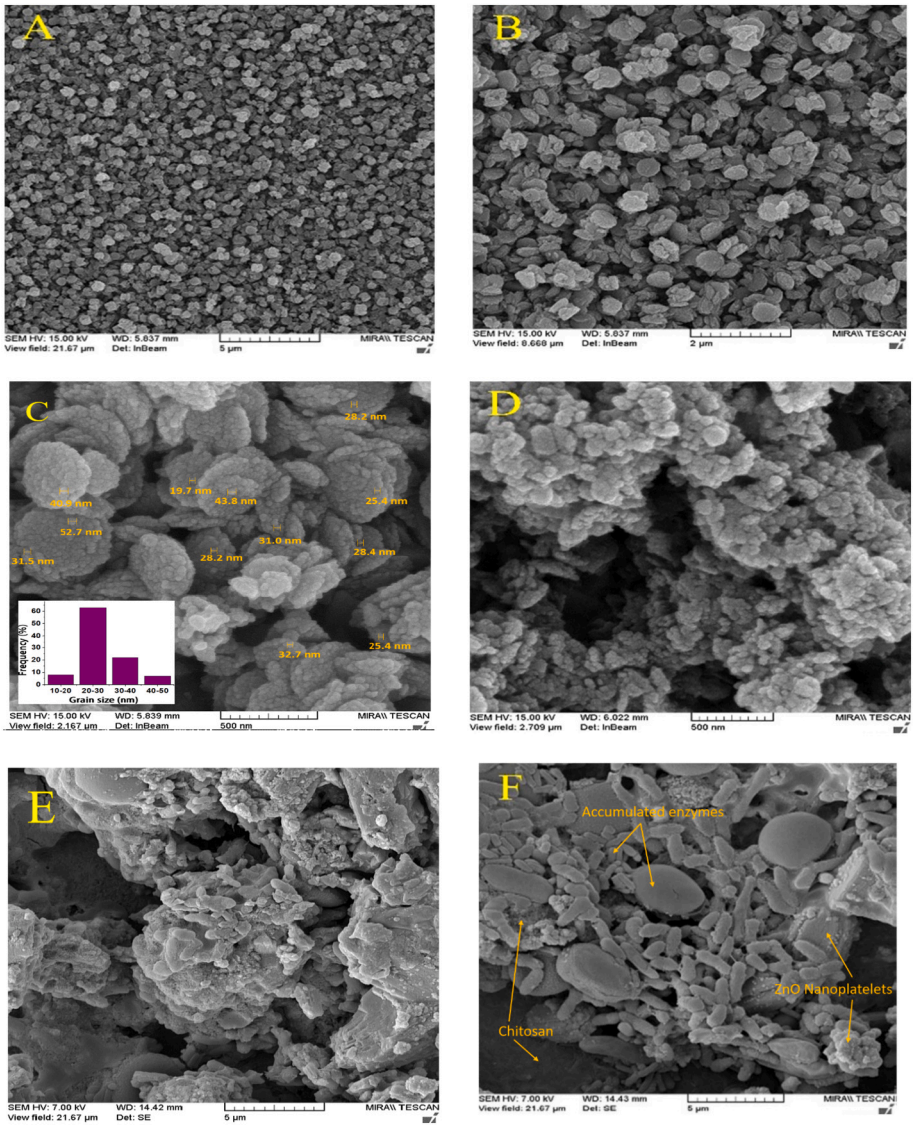

Fig. 2. FE-SEM captures of pre-annealing (A, B, C) and post-annealing (D) FTO/Nano-ZnO/PVA layer, FTO/3D-NPZnO/CTS (E) and FTO/3D-NPZnO/CTS/GOx (F) surfaces. The inset of (C) shows the distribution histogram of the ZnO/PVA grains.

received without any further purification. Potassium phosphate dibasic (K_2HPO_4) and potassium phosphate monobasic (KH_2PO_4) were used for the preparation of phosphate buffer solution (PBS) by precise pH adjusting to the final desired value using HCl or NaOH. D(+)-Glucose stock solution was prepared in PBS (0.1 M, pH = 7.4) and stored at 4 °C. Dilutions from stock solution were prepared at the time of the relevant experiments. FTO (Fluorine-doped SnO_2) coated glass was obtained from Dyesol company. The analysis of the biosensor surface during the fabrication process was followed using a field emission scanning electron microscope (FE-SEM, MIRA II LMH from TESCAN) equipped with an energy dispersive spectroscopy (EDX) analysis detector. Fourier Transform infrared spectroscopy (FTIR) was performed using a Nicolet 60-SXB spectrometer with a resolution of 4 cm^{-1}. A Lambda 3 spectrophotometer (Perkin Elmer, Waltham, MA) was employed for Ultraviolet-Visible (UV–Vis) spectrophotometry, and a Mettler Toledo TGA 850 instrument was used for thermogravimetric analysis (TGA). The BET (Brunauer–Emmett–teller) method was used to calculate the specific surface area of the nano-ZnO/PVA and 3D-NPZnO layers using BET analyzer (BELSORP MINI II, BEL, Japan). Pore size distributions of the nano-ZnO/PVA and 3D-NPZnO layers were obtained from the desorption branch of the Barrett–Joyner–Halenda (BJH) method. Crystalline structures of 3D-NPZnO were analyzed by powder X-ray diffraction (XRD, X'pert, Philips, Holland) using Ni-filtered Cu Kα radiation (λ = 1.5406 A°) in the range of 2θ = 10–80°, step size 0.01°, and time per step 250 s.

Impedimetric and voltammetric experiments were done using a potentiostat/galvanostat (PGSTAT. 302 N, Autolab, Eco-Chemie, the Netherlands) with FRA2 electrochemical impedance spectroscopy (EIS) module. Electrochemical experiments were conducted using a conventional three-electrode system in which fabricated FTO/3D-NPZnO/CTS/GOx biosensor (geometric surface area = 1 cm^2) aided as working electrode, platinum rod (Pt) as the counter, and Ag/AgCl as reference electrodes. For impedance measurements, the applied AC amplitude was 10 mV peak-to-peak, and a range of 100 kHz to 0.01 Hz frequencies was scanned. The obtained data were plotted in the form of Nyquist plot (−Z" *vs.* Z'). Zview/Zplot software (Scribner Associates, Inc.) was employed for the impedance data analysis based on the complex nonlinear least-squares (CLNS) method of Macdonald's LEVM 7 algorithm (Macdonald et al., 1982).

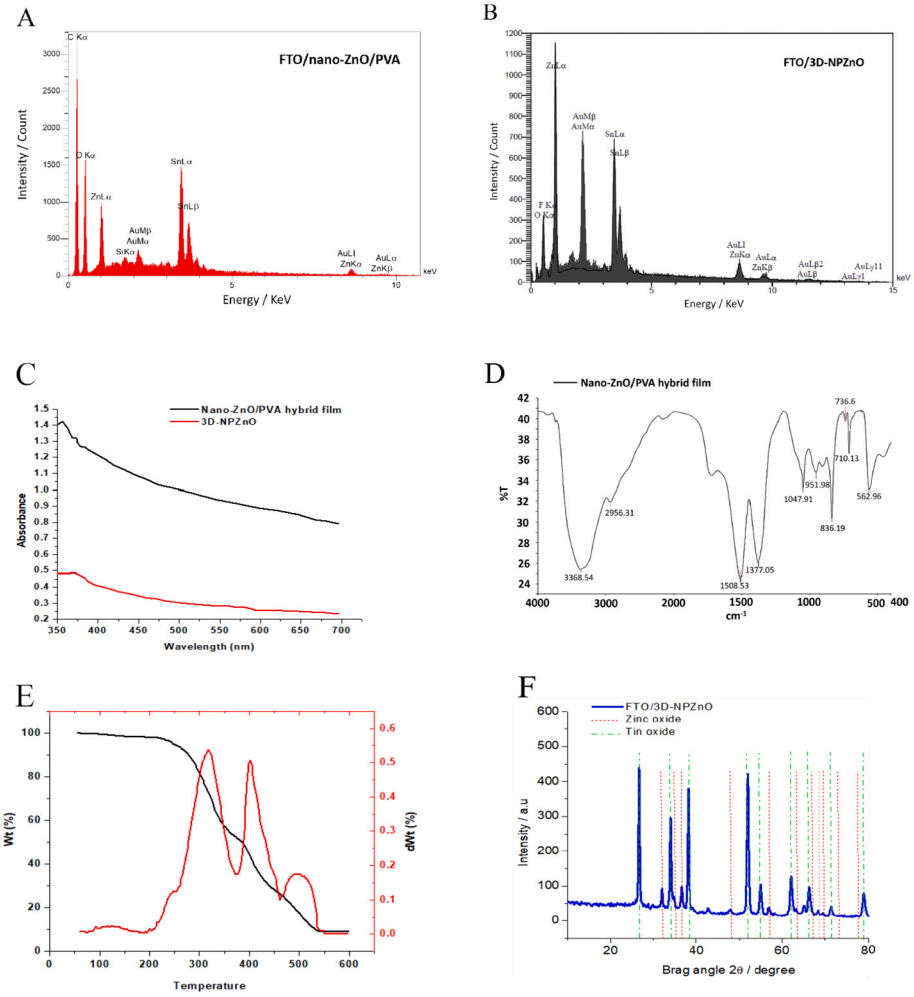

Fig. 3. EDX analysis of nano-ZnO/PVA on FTO substrate (A) before and (B) after annealing; (C) UV-VIS analysis of nano-ZnO/PVA before and after PVA omission; (D) FTIR analysis of nano-ZnO/PVA; (E) TGA and DTG thermogram of nano-ZnO/PVA hybrid film; (F) XRD pattern of 3D-NPZnO on FTO substrate.

2.2. Step by step designing and fabrication of biosensor

Four steps in the surface engineering process of FTO/3D-NPZnO/CTS/GOx fabrication and the reaction mechanism of the fabricated biosensor for glucose sensing are schematically depicted in Fig. 1 and described in the following subsections.

2.2.1. Step (i): fabrication of FTO/Nano-ZnO/PVA hybrid polymeric film by electrodeposition method

To fabricate hybrid polymeric nanocomposite film of nano-ZnO/PVA, FTO coated glasses were sonicated in acetone and ethanol, respectively (5 min in each), washed-out with distilled water, and finished for 2 min in nitric acid (45%) to prepare for the electrochemical deposition. In order to prepare the polymeric electrodeposition solution, a truly homogenized PVA solution (8.0 g/l) was blended with a heated solution of $ZnCl_2$ (0.01 M) and KCl (0.1 M) under vigorous stirring (Pauporté, 2007). After 30 min O_2 gas bubbling, electrodeposition was initiated potentiostatically in an 85 °C thermoregulated bath using FTO, Ag/AgCl, and Pt as working, reference, and counter electrodes, respectively. Then, 20 sets of cyclic potential scan between 0.0 to −1.5 V led to forming nano-ZnO/PVA layer onto the FTO substrate.

2.2.2. Step (ii): construction of FTO/3D-NPZnO surface

In this step, the prepared nano-ZnO/PVA layer was subjected to heat treatment at 430 °C in a furnace for 20 min, which led to the complete removal of the PVA and the formation of 3D-NPZnO with good adhesion on the substrate.

2.2.3. Step (iii) fabrication of FTO/3D-NPZnO/CTS electrode

Chitosan solution was prepared by dissolving 1.0 mg of CTS in 100 ml of 1.0% acetic acid. The FTO/3D-NPZnO electrode was dipped in CTS solution for 10 s and dried at room temperature. The chitosan coating offers a useful hybrid polymeric bio-sensing matrix containing both biocompatible metal oxide (3D-NPZnO) and carbohydrate biopolymer (CTS) for stable enzyme immobilization.

2.2.4. Step (iv): GOx immobilization on FTO/3D-NPZnO/CTS hybrid polymeric matrix

In this step, to immobilize the GOx enzyme, an appropriate amount of a freshly prepared 1.0 mg/ml GOx enzyme solution in PBS (0.1 M, pH 7.4) was placed onto the FTO/3D-NPZnO/CTS surface and allowed to dry at room temperature. The attachment of GOx enzyme with 3D-NPZnO/CTS hybrid film was envisioned to be affected by the dissimilarity in their isoelectric points (p*I*). The fabricated biosensor was then rinsed and stored in PBS under dark at 4 °C until use.

3. Results and discussion

3.1. FTO/3D-NPZnO thin film: structural characterization

The FE-SEM, EDX, UV-VIS, FTIR, and TGA-DTG techniques were exploited to monitor and characterize the biosensor fabrication steps.

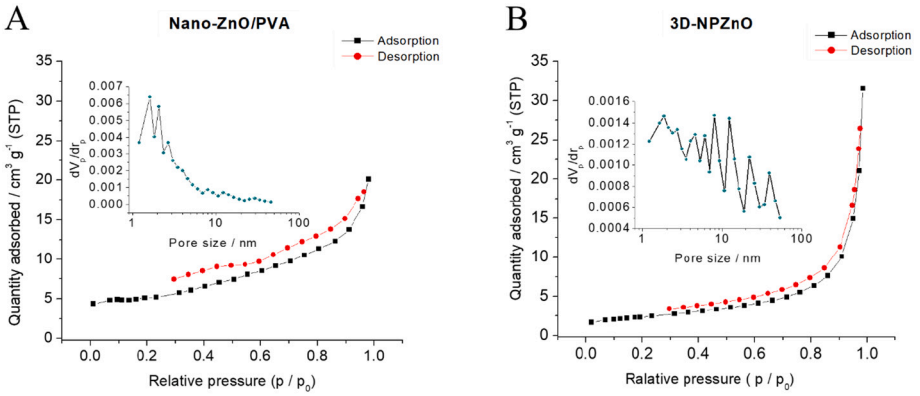

Fig. 4. Nitrogen Adsorption-desorption isotherms and BJH pore size distribution curves (inset) of (A) nano-ZnO/PVA and (B) 3D-NPZnO.

The surface characterization of the nano-ZnO/PVA layer before annealing and at the end of thermal treatment is shown in Fig. 2A–E using the FE-SEM technique. As shown in Fig. 2A–C, in the case of the pre-annealed samples, the nanoplatelets show a smoother and more compact surface than the nanoplatelets whose PVA has been removed by annealing (Fig. 2D). It is difficult to distinguish between components in obtained FE-SEM pictures indicating the close integration of the PVA and ZnO in the fabricated hybrid polymeric film. The size measurement of the ZnO/PVA grains was estimated by Digimizer software and the distribution histogram is shown in Fig. 2C (inset). The length scale of the ZnO/PVA grains was found to be in the range of 10–50 nm with a mean size of about 30 nm.

Some electrochemical reactions primarily govern the overall mechanism for the formation of ZnO thin films during electrodeposition in an aqueous solution and in the presence of oxygen molecules. Briefly, hydroxyl ions produced from the reduction of water and oxygen molecules (Eqs. (1) and (2)) interact with Zn^{2+} ions originated from dissolved $ZnCl_2$ to produce ZnO nanoparticles after hydrolysis (Eq. (3)).

$$2\,H_2O_{(l)} + 2\,e^- \longrightarrow H_{2(g)} + 2\,OH^-_{(aq)} \quad (1)$$

$$O_{2(g)} + 2\,H_2O_{(l)} + 4e^- \longrightarrow 4\,OH^-_{(aq)} \quad (2)$$

$$Zn^{2+}_{(aq)} + 2\,OH^-_{(aq)} \longrightarrow ZnO_{(s)} + H_2O_{(l)} \quad (3)$$

In the PVA-assisted electrodeposition of ZnO, it is known that the presence of PVA as a polymeric additive strongly affects the growth mechanism of ZnO nanoparticles through interaction with Zn^{2+} ions and ZnO species and thus changes the preferential growth axis of ZnO crystals (Kumar et al., 2003; Pauporté, 2007; Yang, Shao, et al., 2004).

Fig. 2D and E illustrate the morphology of obtained 3D-NPZnO film after annealing of nano-ZnO/PVA layer and 3D-NPZnO/CTS film, respectively. It is evident from FE-SEM images that the particle sizes of nanostructured ZnO film were reduced. These pieces of evidence suggest that the removal of the PVA polymer from the nano-ZnO/PVA layer creates a uniform distribution of open pores which are exposed to the bulk and is believed to play an essential role in increasing the subsequent microenvironment for enzyme loading and thus improving the biosensor characteristics such as responses and biosensitivity. Further, the nano-size distribution of ZnO metal oxide particles provides a high surface area nanostructured matrix for chitosan layer formation and a more immobilization of GOx enzyme on the surface. The presence of different particles at the enzyme loaded 3D-ZnO/CTS surface was indicated in Fig. 2F, which clearly shows accumulated enzymes, chitosan layer, and ZnO nanoplatelets.

Based on these observations, the hierarchical 3D-NPZnO/CTS can serve as a promising platform to provide high loading and stable enzyme immobilization. Ang et al. (Ang et al., 2013) investigated this interesting simple immobilization of proteins such as enzymes in the chitosan biopolymeric carbohydrate network by a precise comparison of the FTIR spectra for GOx enzyme and GOx-chitosan layer. They reported that the formation of intermolecular hydrogen bonds between the abundant amine groups of chitosan and the enzyme molecules is the reason for this stable GOx-chitosan bonding.

Fig. 3A and B show the EDX analysis of ZnO/PVA film before and after annealing. The presence of oxygen, fluorine, tin, and zinc peaks confirm the formation of the ZnO layer on the fluorinated SnO_2 substrate. The comparison of the two EDX spectra shows that the removal of carbon from surface layers is almost completed after the annealing process.

Fig. 3C depicts the recorded UV–Vis absorption spectrum in the wavelength range of 350 to 700 nm for the ZnO and nano-ZnO/PVA layer, respectively. The lower absorption values of the 3D-NPZnO layer exhibit PVA omission during thermal treatment of the nano-ZnO/PVA layer.

The FTIR spectrum of nano-ZnO/PVA film is shown in Fig. 3D. The broad absorption band between 3450 and 3210 cm^{-1} is due to the O—H stretch modes of intramolecular and intermolecular hydrogen bonds. The vibrational band emerging at 2956 cm^{-1} represents the C—H stretching vibration from alkyl groups of PVA, even though after thermal treatment and PVA elimination, neither stretching absorption bands nor vibrational bands were observed (Andrade et al., 2006; Coates & Meyers, 2000). These pieces of evidence confirm the hybrid nature of the fabricated nano-ZnO/PVA film. PVA has a carbon chain backbone with hydroxyl groups, which is the polar part and can form electrostatic interaction may be in the form of hydrogen bonding with the zinc oxide leading to a strong interfacial interaction (Barman et al., 2019).

Thermogravimetric analysis (TGA), together with differential thermal analysis (DTG), were employed to assess the thermal durability and ascertain the breaking apart temperature of PVA films. The range of the studied temperatures was 30 °C to 600 °C at a heating rate of 5 °C/min under the atmosphere of nitrogen gas. Fig. 3E displays the overlay of the TGA thermogram and DTG graph of the nano-ZnO/PVA film with three-step weight loss. The first occurs in the temperature range of 80–200 °C, which corresponds to the removal of the physically adsorbed water. The decomposition process occurred at 215–375 °C is attributed to the amorphous parts of the PVA decomposition. This stage is followed by a second degradation stage between 375 and 465 °C, which is due to the PVA crystalline parts decomposition, likely via breakdown of the polymer backbone by a dehydration reaction and carbon/hydrocarbon yield. Complete degradation of the polymer at 465–549 °C can be ascribed to the break of NP-ZnO/PVA links (Peng & Kong, 2007). As shown in Fig. 3E, after TGA analysis, whole PVA content in the ZnO/PVA is expected to be removed, leaving a white ZnO powder (less than 10% by weight).

The XRD pattern of the ZnO layer grown on FTO coated glass is shown in Fig. 3F. As compared to standard Zincite (wurtzite structure,

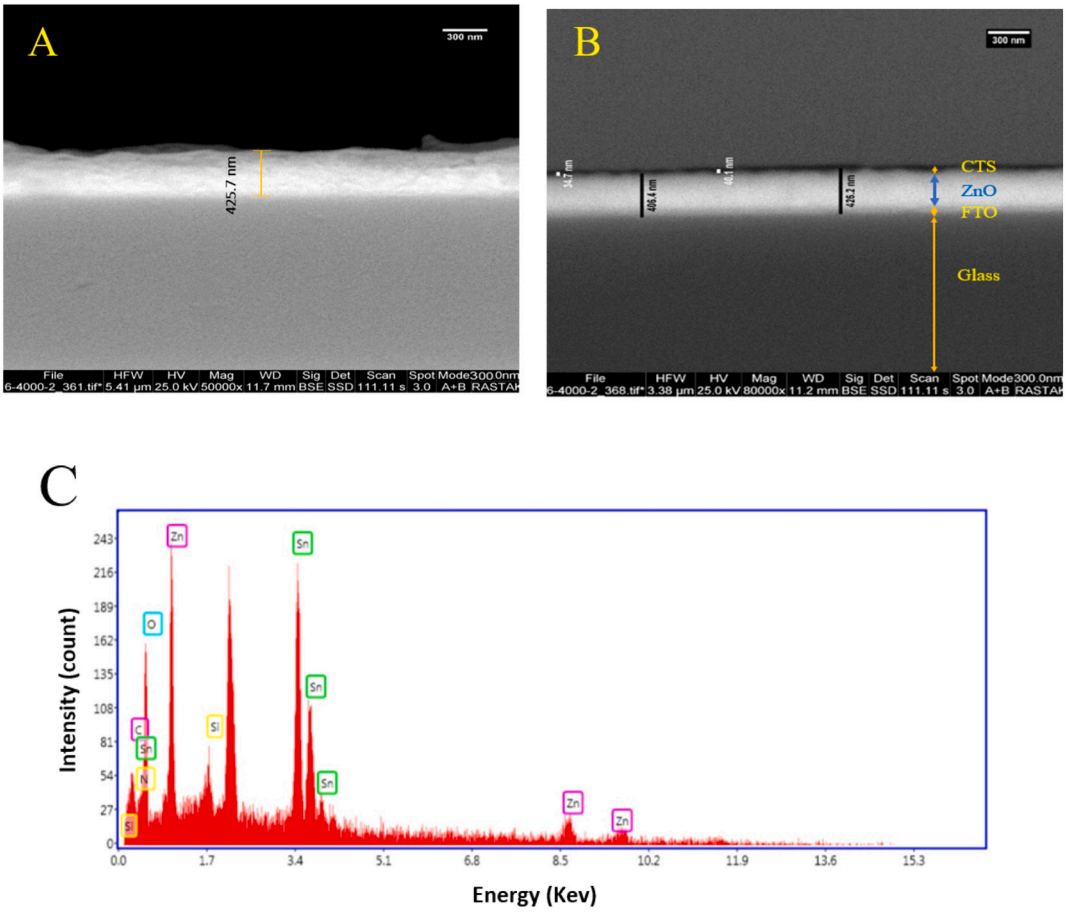

Fig. 5. Cross-sectional FE-SEM of FTO/Nano-ZnO/PVA (A) and FTO/3D-NPZnO/CTS (B) layers, EDX analysis of the fabricated FTO/3D-NPZnO/CTS electrode (C).

Card JCPDS: 01–075-1526), the peaks depicted with red dotted lines correspond to the characteristic peaks of hexagonal wurtzite structure of ZnO.

3.2. BET and BJH measurements

The mesoporosity of the ZnO/PVA before and after annealing was characterized by Brunauer-Emmett-Teller (BET) surface area analysis and Barrett-Joyner-Helena (BJH) pore size analysis (Fig. 4 A, B). The specific surface area of the annealed ZnO/PVA (as 3D-NPZnO) was obtained 13.22 $m^2\ g^{-1}$, which is higher than 8.26 $m^2\ g^{-1}$ obtained for the non-annealed ZnO/PVA. Furthermore, as can be seen from Fig. 4 A, B (insets), the annealed ZnO/PVA compare with the non-annealed ZnO/PVA shows a multimodal pore size distribution, which is suggested to be due to the simultaneous formation of versatile porous and dislodging of PVA.

3.3. Investigation of chitosan film formation onto the FTO/3D-NPZnO surface

Enzyme immobilization is considered a crucial aspect to design practical biosensors with suitable capabilities such as storage steadiness, quick response time, high selectivity, sensitivity, and reproducibility. Chitosan is a biocompatible, non-toxic polymer exploited in the preparation of biosensors as functional support to adsorb enzymes with unique polycation properties and excellent film-forming ability. Since CTS is produced via semi-deacetylation of chitin chains, it can be considered as a *co*-polymer of *N*-acetyl-D-glucosamine and D-glucosamine. As far as known, there is no nature-derived polymer with such amine-richness. Many of the beneficial functional properties of chitosan that are especially important for the development of the biodevice interfaces are provided by these amine groups.

Chitosan has pH-responsive properties due to the presence of amine groups. At low pH, the protonation of CTS's primary amines results in a soluble cationic polyelectrolyte solution. At high pH, deprotonation of these amine groups makes CTS insoluble. Importantly, as soluble to insoluble transitions of CTS occurs near its pk_a ($\approx$ 6), therefore the biosensor surface remains insoluble at the biological pH (7.4) during the experiments.

The CTS film formation on the 3D-NPZnO surface and bond formation between them depends on the ability of the CTS molecules to overcome electrostatic and steric repulsion forces and the accessibility of chitosan chains for hydrogen bonding. Besides, the mobility of chitosan chains highly depends on pH, which can make the chains rigid or mobile (Chen et al., 1996; Xu et al., 2005). At the film formation pH (acidic media), the chitosan surface becomes positive through the protonation of chains, which may cause repulsion of positively charged ZnO nanostructures; however, hydrogen bonding and van der Waals forces overcome the repulsions, and chitosan film successfully forms on the surface. Cross FE-SEM images obtained for FTO/ZnO/PVA (Fig. 5A) and FTO/3D-NPZnO/CTS surface (Fig. 5B) confirm the formation of a CTS thin layer with a thickness of approximately 40 nm onto the 3D-NPZnO thin film with a thickness of about 400 nm. This thickness is large enough to anchor the enzyme in a stable manner, while due to its low thickness, it does not prevent electron and ion transfer across the chitosan layer. Also, the EDX analysis of FTO/3D-NPZnO/CTS surface (Fig. 5C) shows the presence of nitrogen and carbon atoms as proof for the formation and presence of the CTS layer at the FTO/3D-NPZnO

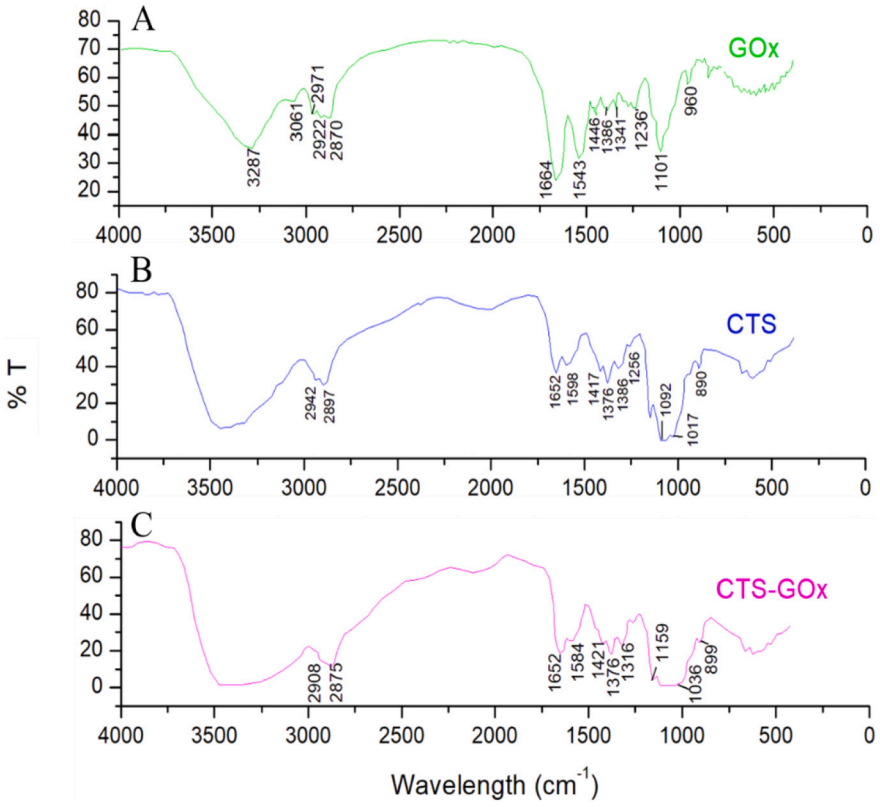

Fig. 6. FTIR Spectra of (A) GOx, (B) CTS and (C) CTS-GOx hybrid film.

surface.

Four types of crystal structures, including extended 2-fold helix, relaxed 2-fold helix, 4/1 helix, and 5/3 helix, have been identified for chitosan depending on the local environment (Ogawa et al., 2004). As the two former structures (4/1 helix and 5/3 helix) only occur in the presence of iodide ions and aromatic organic acids, respectively, therefore, chitosan prefers to have a 2-fold helix structure in acetate buffer systems (Kawahara et al., 2003; Lertworasirikul et al., 2003). In this condition, chitosan does not include strong intramolecular hydrogen bonds and exposes many protonated amine groups incorporated in hydrogen bond formation with oxygen atoms of ZnO thin film (Okuyama et al., 2000).

3.4. FTIR investigation of the CTS and CTS-GOx layers

To investigate the interaction of GOx enzyme with chitosan layer through immobilization, the FTIR technique was used as a powerful tool for monitoring the types and changes of chemical bonds. Fig. 6 displays the spectra of GOx crystal, chitosan, and the glucose oxidase immobilized on the CTS layer. As can be seen in Fig. 6A, the crystalline GOx spectrum shows two strong peaks at 1739 cm^{-1} and 1626 cm^{-1}, which are respectively attributed to the C═O stretching and N—H bending vibration of the amide bonds. The peaks between 1376 cm^{-1} and 1445 cm^{-1} are assigned to symmetric and asymmetric vibrations of COO^- groups, and the absorption bands at 2866 cm^{-1} and 2874 cm^{-1} are attributed to symmetric and asymmetric vibrations of CH_2 groups, respectively. Also, the strong band observed at 3281 cm^{-1} and a weaker band at 3067 cm^{-1} are attributed to amide bands of GOx enzyme (Wang et al., 2017).

As shown in Fig. 6B, the FTIR spectra of the chitosan layer is similar to the GOx-CTS (Fig. 6C), with small differences in the absorption intensities and range of frequencies. The absorption bands at 1376–1445 cm^{-1} region (Fig. 6C) represent the overlapping of the GOx vibrational modes with the CH_3 bending bands of the CTS layer (Branca et al.,

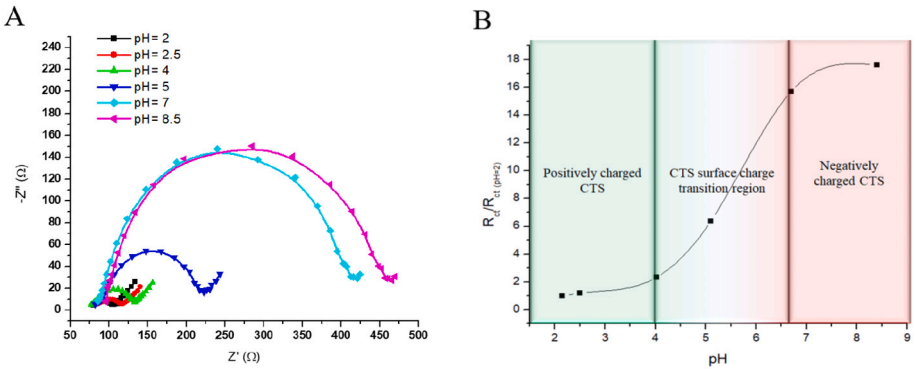

Fig. 7. Nyquist plots (A) and impedimetric pH titration graph (B) using FTO/3D-NPZnO/CTS as the working electrode and $[Fe(CN)_6]^{3-/4-}$ as a negative redox probe in pH range from 2 to 8.5.

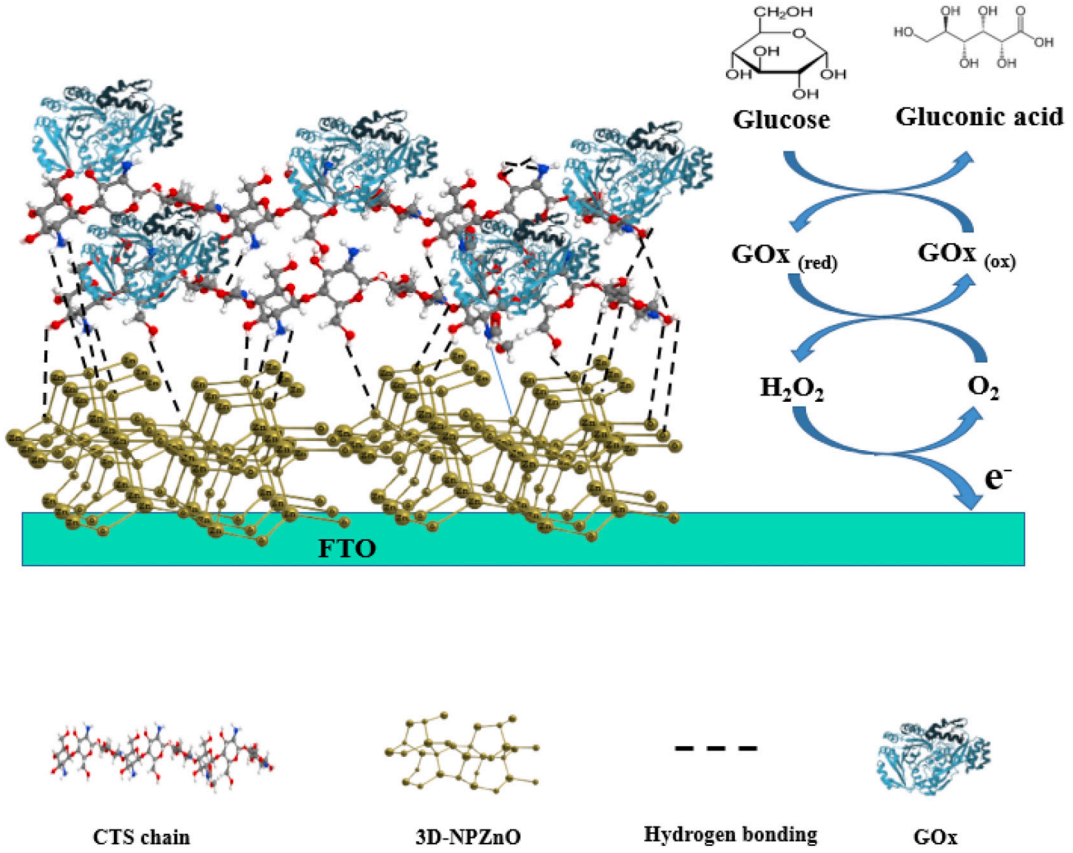

Fig. 8. Schematic representation of the fabricated FTO/3D-NPZnO/CTS/GOx electrode and charge transfer between the glucose and electrode surface through the CTS as a polyelectrolyte.

2016).

The absorption bands at 1000–1100 cm^{-1} in the spectrum of GOx-CTS film (Fig. 6C) appeared as a characteristic absorption spectrum typical of the phosphate buffer, which has been used for the preparation of the enzyme solution. Furthermore, intermolecular hydrogen bonds between chitosan and GOx molecules result in a broad band of O—H stretching at 3200–3600 cm^{-1} (Yang, Wang, & Tan, 2004). The peak at 1545 cm^{-1} in the spectrum of crystalline GOx was assigned to strong N—H bending vibration of the secondary amide. The vanishing of the peak at 1545 cm^{-1} may be attributed to the interaction of CTS with GOX and the N—H deformation of primary amines (Melo et al., 2013).

3.5. Investigation of the surface charge potential of the CTS layer

To determine pK_a of chitosan surface and bring in a clear understanding of the surface charge potential at different pHs, impedimetric pH titration (Mozaffari et al., 2009) was performed using fabricated FTO/3D-NPZnO/CTS as working electrode and $[Fe(CN)_6]^{3-/4-}$ as a negative redox probe. The results are shown in Fig. 7A, B, while R_{ct} is a demonstration of the negative charge potential of the surface. In lower pHs ($2 < pH < 4$), surface has a positive charge due to protonation of amine groups of CTS; so, R_{ct} is low. As the negative charge of the surface increases ($pH > 4$), the negative charged $[Fe(CN)_6]^{3-/4-}$ probe is repelled strongly from the electrode surface, and as a result, R_{ct} increases dramatically. At a pH of about 6.0, an inflection point can be seen, which means that the negative surface charge after this pH is dominant due to deprotonation of CTS chains functional groups.

Consequently, in biological pH (7.4), the negatively charged FTO/3D-NPZnO/CTS can be used as a favorable microenvironment for high enzyme anchoring through electrostatic adsorption, which is induced by the difference in CTS and GOx surface charges. Fig. 8 illustrates the schematic diagram of the hierarchical arrangement of fabricated biosensor and the charge transfer of the enzymatic redox reaction to 3D-NPZnO surface through the CTS as a mediator polyelectrolyte. The way that the cast chitosan layer with different thicknesses or with an additional salt can provide an electrolytic interface between the deposited zinc oxide nanoparticles and the glucose oxidase enzyme of the glucose sensor is an exciting issue in terms of describing the interface effect. The thickness of the chitosan layer should be small enough to provide high conductivity, and on the other hand, it should be thick enough to allow the enzyme to bind and locate easily. The ionic conductivity of the chitosan layer can be provided in various ways: when a chitosan layer is swollen in water, the amino groups may be protonated, leaving the hydroxide ions free in the water, which may contribute to the ionic conduction in the membrane, named as intrinsic ionic conduction. Furthermore, during the preparation of chitosan film in acetic acid media, the acetate ions, which have been anchored in some of the amino groups, lead the mobility of both hydroxide and hydronium through ion-ion Colombian type interactions (López-Chàvez et al., 2006). Besides, doing the biosensing experiments in the electrolyte of phosphate-buffered solution causes an increase in the system's total conductivity. Accordingly, it is possible to imply that the mechanism for ionic conductivity through the membranes may come from the function of free amine groups in the chitosan backbone or the mobility of the charge carrier ionic species in the chitosan layer (Wan et al., 2003).

3.6. Activity determination for immobilized enzyme

In an attempt to determine the enzyme activity after immobilization onto 3D-NPZnO/CTS hybrid polymeric matrix, the electrical feature of the FTO/3D-NPZnO/CTS transducer and FTO/3D-NPZnO/CTS/GOx biosensor was examined in a two electrodes cell using a gold wire

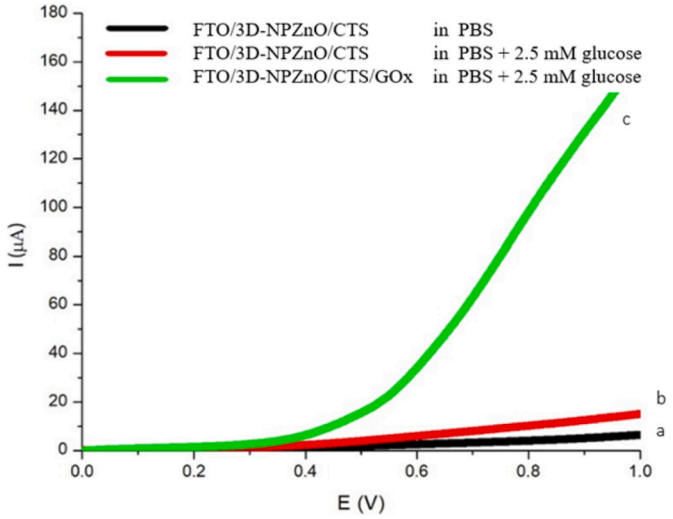

Fig. 9. Effect of GOx immobilization on 3D-NPZnO/CTS films. I-V curves for the FTO/3D-NPZnO/CTS electrode in (a) PBS, (b) PBS (pH 7.4, 0.1 M) containing 2.5 mM glucose before and (c) after GOx immobilization.

(0.3 mm in diameter and 5 cm in length) as anode and the fabricated biosensor as the cathode. A certain concentration of substrate (glucose in this case) was added to a constant volume of PBS electrolyte (10 ml), and a sweep scan of potential was performed in the range of 0.0 to 1.0 V. Under the applied potential, the proportional DC current response was recorded (Fig. 9) in the presence and absence of glucose, and the voltage to current ratio was considered as a measure of enzyme activity (Mozaffari et al., 2014). The effect of introducing glucose to the solution on the slope of recorded I—V curves is related to the enzyme activity and, as a result, to biosensor sensitivity (Ansari et al., 2008; Mahadeva & Kim, 2011).

As evidenced in Fig. 9, dramatic changes in I-V characteristics were observed after GOx immobilization, which proves the enzyme's high activity after immobilization on the 3D-NPZnO/CTS hybrid polymeric matrix. The high performance of the FTO/3D-NPZnO/CTS/GOx can be due to the high surface to volume ratio of 3D-NPZnO/CTS hybrid film, which can act as an adequate microenvironment for enzyme immobilization. The efficiency (%) of GOx immobilization onto the FTO/3D-NPZnO/CTS for the reported conditions in section 2.2.4., was obtained as 68.2% from the following equation (Mohamed et al., 2017):

$$\text{Immobilization efficiency } (\%) = \frac{\text{Activity of immobilized enzyme}}{\text{Initial activity of soluble enzyme}} \times 100 \quad (4)$$

The immobilized GOx molecules on 3D-NPZnO/CTS film can bio-electrocatalyze the conversion of glucose to gluconic acid, and then retrieve by donating electrons to oxygen molecules and as a result hydrogen peroxide (H_2O_2) will be produced. The final step comprises free electrons production through the dissociation of a single oxygen-oxygen bond of hydrogen peroxide. The resulting output signal of the biosensor is an electric current obtained by sensing these electrons (Marie et al., 2015; Yang et al., 2009). Three steps of the GOx-glucose reaction mechanism are summarized in the following equations:

$$\text{Glucose} + \text{GOx}_{(\text{Ox})} \rightarrow \text{Gluconic acid} + \text{GOx}_{(\text{Red})} \quad (5)$$

$$\text{GOx}_{(\text{Red})} + \text{O}_2 \rightarrow \text{GOx}_{(\text{Ox})} + \text{H}_2\text{O}_2 \quad (6)$$

$$\text{H}_2\text{O}_2 \rightarrow \text{O}_2 + 2\text{H}^+ + 2\text{e}^- \quad (7)$$

3.7. Response behavior of FTO/3D-NPZnO/CTS/GOx biosensor in the presence of $[Fe(CN)_6]^{3-/4-}$ redox probe

Detailed investigations of FTO/3D-NPZnO/CTS/GOx fabrication steps were performed by employing CV and EIS electrochemical methods. For this purpose, the electrical response of the electrode at each step was monitored by following the magnitudes of anodic peak current (i_{pa}) from CV voltammograms and charge transfer resistance (R_{ct}) from Nyquist plots in a glucose-free solution of 5 mM $[Fe(CN)_6]^{3-/4-}$ redox pair (Fig. 10A and B). The amounts of i_{pa} and R_{ct} change from i_{pa} = 1.10 mA and R_{ct} = 0.85 kΩ, curve a, for FTO layer to i_{pa} = 0.40 mA and R_{ct} = 1.75 kΩ, curve b, for FTO/3D-NPZnO, and i_{pa} = 0.20 mA, R_{ct} = 3.54 kΩ, curve c, for FTO/3D-NPZnO/CTS/GOx, respectively. The observed increase in R_{ct} and decrease in i_{pa} values of the 3D-NPZnO film (Fig. 10A and B, curve b) against the FTO electrode (Fig. 10A and B, curve a), as well as further changes for immobilized GOx enzyme (Fig. 10A and B, curve c), was referring to the higher resistance of the fabricated 3D-NPZnO film and insulating characteristics of CTS/GOx matrix.

3.8. Response behavior of FTO/3D-NPZnO/CTS/GOx biosensor in the presence of glucose

In this research work, the physiological pH (pH = 7.4) was selected for the glucose measurement since the GOx enzyme exhibits its high activity at this pH. Sustaining the three-dimensional structure of the enzyme is important to preserve its efficient performance and, consequently, improve the analytical performance of glucose sensing in terms of enhancing the sensitivity and reducing the detection limit. Chitosan provides a positive net charge surface, which electrostatically attracts the negatively charged GOx (pI = 4.2) at physiological pH, so in combination with 3D-NPZnO, it provides a highly efficient microenvironment for GOx enzyme immobilization.

Fig. 11A and B shows the cyclic voltammograms and the Nyquist

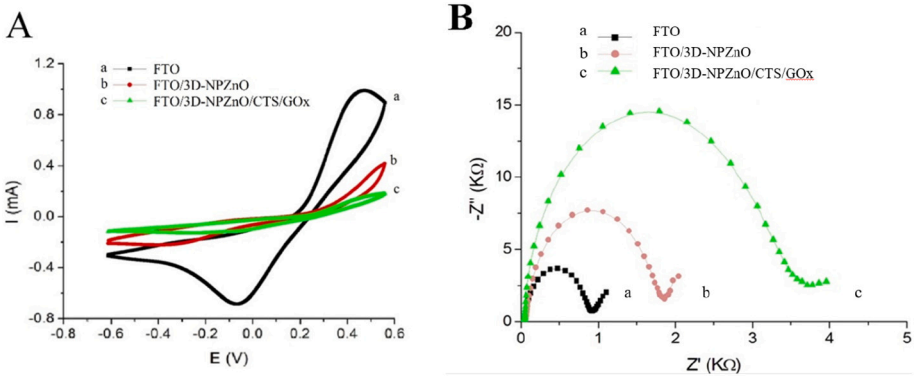

Fig. 10. (A) The cyclic voltammograms (scan rate 0.1 V/s), and (B) Nyquist plots (−Z" vs. Z') for FTO, FTO/3D-NPZnO, and FTO/3D-NPZnO/CTS/GOx in glucose-free PBS (pH 7.4, 0.1 M) containing 5 mM $[Fe(CN)_6]^{3-/4-}$ as redox probe.

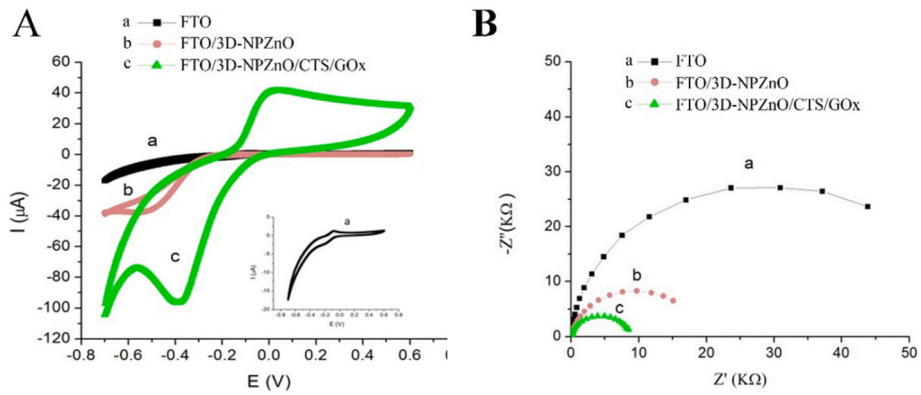

Fig. 11. (A) The cyclic voltammograms (scan rate 0.05 V/s), and (B) Nyquist plots (−Z" *vs.* Z') for FTO, FTO/3D-NPZnO, and FTO/3D-NPZnO/CTS/GOx in PBS (0.1 M, pH 7.4) containing 2.0 mM glucose.

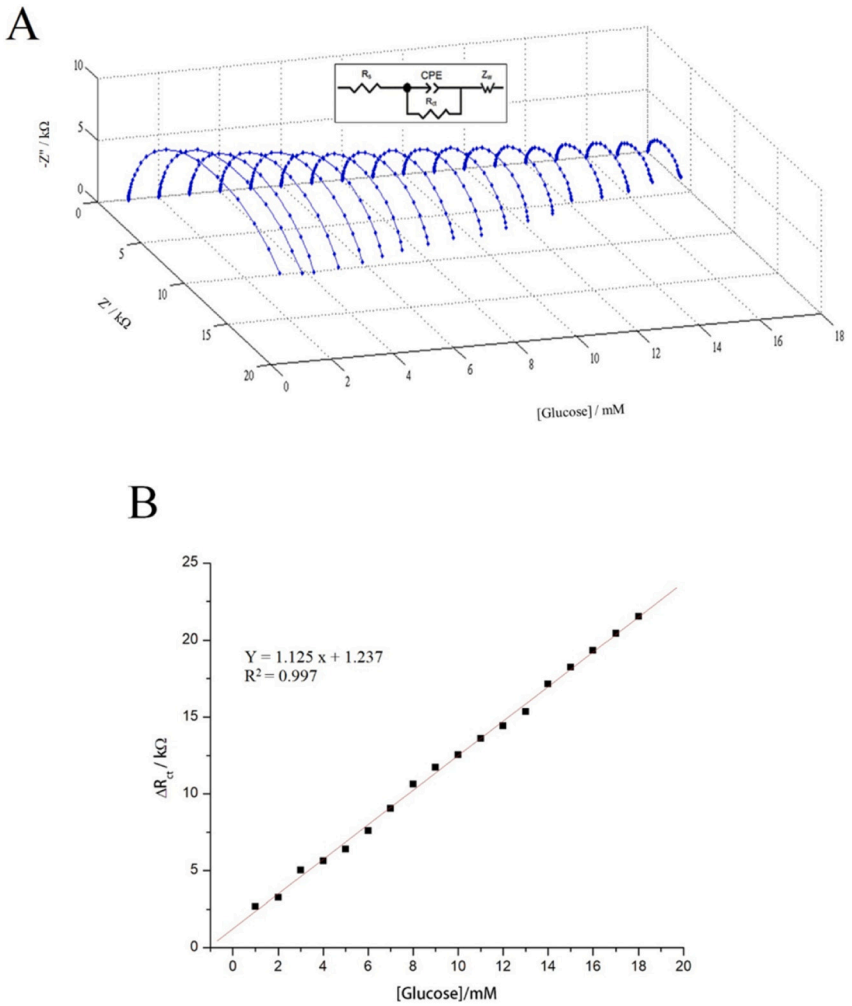

Fig. 12. (A) Nyquist plots achieved for FTO/3D-NPZnO/CTS/GOx glucose biosensor in PBS (pH 7.4, 0.1 M) containing 1.0–18.0 mM glucose (inset shows the modified Randles equivalent circuit used for impedance data approximation), and (B) calibration curve related to the changes in charge transfer resistance (ΔR_{ct}) as a function of variation in glucose concentration.

plots of biosensor preparation stages, which were recorded in 2.0 mM glucose containing PBS (0.1 M, pH 7.4). The i_{pa} and R_{ct} values at 3D-NPZnO film (i_{pa} = 3.0 μA, R_{ct} = 21.13 kΩ) in comparison to the FTO electrode (i_{pa} = 2.0 μA, R_{ct} = 61.01 kΩ) might be related to the partial oxidation of glucose at the 3D-NPZnO film. A further increase in anodic peak current and decrease in charge transfer resistance values (i_{pa} = 42.0 μA, R_{ct} = 9.01 kΩ) after the GOx immobilization onto the FTO/3D-NPZnO/CTS electrode was observed, which can be ascribed to the rapid bioelectrocatalytic oxidation of glucose by the enzyme.

Table 1
Glucose concentration assessment in blood serum.

Sample number	Determined by spectrophotometry (mM)	Measured by FTO/3D-NPZnO/CTS/GOx biosensor (mM)	R.S·D.[a] (n = 5) (%)
1	5.05*	5.03	1.92
2	6.27	6.22	3.53
3	4.94	5.00	5.80
4	5.49	5.52	3.44

[a] R.S.D.: Relative Standard Deviation.
* Normal concentration of blood glucose range is from 4.4 to 6.6 mM (Wang, 2008), and the glucose concentration in patients with diabetes is above 7.0 mM (Dai et al., 2007).

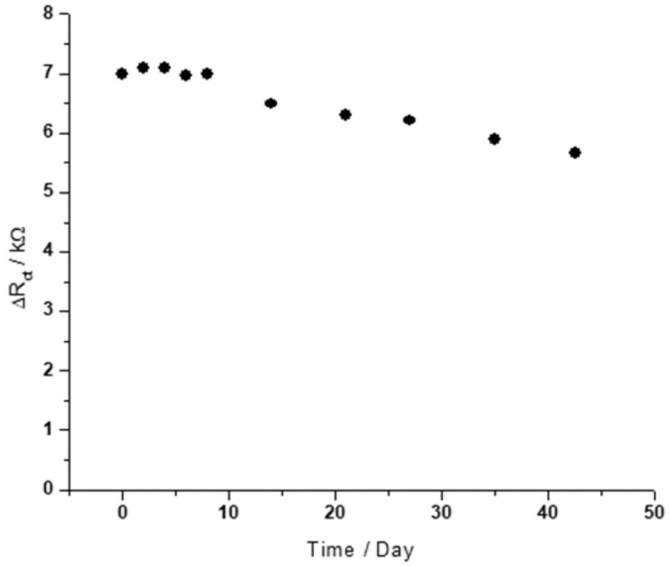

Fig. 13. Long-term stability of the fabricate FTO/3D-NPZnO/CTS/GOx biosensor.

3.9. Impedimetric measurements of glucose using FTO/3D-NPZnO/CTS/GOx biosensor

Electrochemical impedance spectroscopy (EIS) is a highly reliable, informative technique, which is practical to track alterations in interfacial properties by following electrical signal changes stemming from biorecognition events at the modified electrode surfaces (Mozaffari et al., 2010; Shervedani et al., 2006; Shervedani & Mozaffari, 2006). The impedimetric response of the fabricated FTO/3D-NPZnO/CTS/GOx glucose biosensor as a function of glucose concentration has been measured. Fig. 12A shows a typical impedimetric response of the fabricated glucose biosensor to the successive 1.0 mM increments of glucose. As indicated by the results, increasing the concentration of glucose in the range of 1.0 to 18.0 mM leads to decreased charge transfer resistance. The response time of the fabricated biosensor to the glucose concentration is less than 4 s, signifying the FTO/3D-NPZnO/CTS/GOx biosensor's exceptional catalytic characteristics. The impedimetric repetition measurements strongly candidates the fabricated biosensor as a reusable impedimetric biosensor for glucose detection.

EIS data approximation for quantitative impedimetric glucose detection was performed using the modified Randles equivalent circuit model (Fig. 12A inset). A chi-square factor (χ^2) less than 10^{-3} was considered as an acceptable error for any performed approximation. By calculating the R_{ct} values, a calibration curve was developed for glucose determination by applying the fabricated biosensor in a concentration range of 1.0 to 18.0 mM (Fig. 12B). The calibration equation was: ΔR_{ct} (kΩ) = 1.125 [Glucose] (mM) + 1.237; R^2 = 0.997; where $\Delta R_{ct} = R_{ct\ buffer\ (blank)} - R_{ct\ glucose}$. Also, the detection limit of 0.2 mM and a sensitivity of 1.125 kΩ mM^{-1} were obtained for glucose determination using the developed biosensor.

To test the accuracy of the glucose measurement using the fabricated biosensor, several assays were conducted in blood serum samples, and the obtained results were compared with the measured values using spectrophotometry technique at a local clinic. The results showed a good correlation between the values obtained using the prepared sensor and the spectrophotometric method, which indicates the excellent precision, accuracy, and usability of the fabricated biosensor in the real biological sample measurements (Table 1).

3.10. Investigation of the FTO/3D-NPZnO/CTS/GOx biosensor stability

For the investigation of the biosensor stability, the impedimetric response of the FTO/3D-NPZnO/CTS/GOx biosensor to the concentration of 5 mM glucose solution was measured every two days for eight days. After that, measurements were carried out weekly. Each measurement was replicated three times, and the average of the measurements was plotted. Between the measurements, the biosensor was stored at 4 °C in a refrigerator. The results are shown in Fig. 13. In the first eight days, no obvious change in the recorded signal was observed. After one month, the signal decreased to approximately 90% of the initial value, and after six weeks, the sensor maintained 83% of the response. The good stability of the fabricated glucose biosensor can be assigned to the stability of the 3D-NPZnO/CTS and the effective anchoring of GOx on its biocompatible micro-environment, which prevents enzyme leakage.

Finally, the biosensing characteristics of the fabricated biosensor compared with some other reported polymeric glucose biosensors are summarized in Table 2. As shown, developing glucose biosensors through electrostatic enzyme immobilization strategy and using the impedimetric method for assessment showed satisfactory efficacy compared with the other enzyme-based biosensors. The proposed biosensor represented fast response time, low detection limit, and good linear range.

4. Conclusions

The unique properties of polyvinyl alcohol and chitosan were exploited in the development of a novel impedimetric glucose biosensor by (i) fabrication of a unified 3D-nanoporous ZnO film using polymer-supported electrodeposition of ZnO to form nano-ZnO/PVA hybrid film followed by PVA removal via heat treatment, (ii) coating a chitosan layer as biopolymer supporting layer on 3D-nanoporous ZnO film to prepare hierarchical 3D-NPZnO/CTS microenvironment for enzyme immobilization, (iii) electrostatic immobilization of GOx on the 3D-NPZnO/CTS surface based on the dissimilarity in enzyme and substrate isoelectric points. Regarding the crucial role of chitosan in mediating enzymatic redox reaction at the biosensor surface, several important parameters were investigated such as the chitosan film formation and its thickness, charge potential of casted chitosan film, the type of enzyme interactions with chitosan film, and enzyme activity after immobilization. By exploiting unique properties of impedimetric technique, including rapidity, sensitivity, and repeatability, in combination with outstanding characteristics of the abovementioned polymers, the fabricated biosensor showed exceptional analytical performance for glucose detection.

CRediT authorship contribution statement

Sahere Khazaei: Conceptualization, Methodology, Software, Data curation, Writing – original draft. **Sayed Ahmad Mozaffari:** Supervision, Conceptualization, Writing – review & editing. **Fateme Ebrahimi:** Conceptualization, Methodology, Software, Validation, Writing – review & editing.

Table 2
Analytical characteristics of FTO/3D-NPZnO/CTS/GOx biosensor compared with some of the other reported polymeric glucose biosensors.

Polymer-based matrix	D.R[a] (mM)	D.L[b] (mM)	S[c] ($\mu A\ mM^{-1}\ cm^{-2}$)	R. T[d] (s)	R[e] (%)	Polymeric base	Method	Ref
PMMA–BSA particles	0.2–9.1	–	44.1	< 8	–	PMMA	Amperometry	(He et al., 2012)
Au NPs/PPY/RGO/GOD/CS	0.2–1.2	–	123.8	–	–	PPY	Amperometry	(Xue et al., 2014)
CTS/CAR PEC chitosan/κ-carrageenan polyelectrolyte complex	0.005–7	0.005	–	–	–	Chitosan-κ-carrageenan	SWV	(Rassas et al., 2019)
Chitosan/GOx/ZnONRs/ITO	0.01–0.04	0.01	–	–	–	Chitosan	CV	(Bagyalakshmi et al., 2020)
MPC-CTS-GOx	0.25–3	0.004	56.12	–	3.6	Chitosan	Amperometry	(Barathi et al., 2019)
CS/GLM/GCE	0.01–10	0.01	2.0	–	–	Chitosan	Amperometry	(Guan et al., 2019)
Pt/Double CTS layer/GOx	0.05–15	0.01	21	< 8	4.2	Chitosan	Amperometry	(Yang, Yang, et al., 2004)
GOD/ZnO/CTS-g-PVA/ITO	0.002–1.2	2.0×10^{-4}	>0.04 V μM^{-1}	3	–	Chitosan - PVA	Potentiometric	(Shukla et al., 2012)
GOx/MWCNTs-CTS/GCE	0.2–1.2	0.05	1.31	–	–	Chitosan	DPV	(Uwimbabazi et al., 2017)
Chitosan cryogel	0.3–3.0	0.3	38.31 intensity mM^{-1}	600	–	Chitosan	Colorimetry	(Fatoni et al., 2019)
PPY/GOx/AuNPs/GR	–	0.20	21.7	5	–	PPY	Amperometry	(German et al., 2017)
Poly(2,6-DP)/MWCNT/GCE	4.2×10^{-5} - 8.0	4.2×10^{-4}	52.0	–	1.6	DAP	CV	(Kamyabi et al., 2013)
FTO/3D-NPZnO/CTS/GOx	1.0–18.0	0.20	1.125 $k\Omega\ mM^{-1}\ cm^{-2}$	< 4	3.5	Chitosan & PVA	Impedimetric	This work

[a] Detection range.
[b] Detection limit.
[c] Response time.
[d] Sensitivity.
[e] Repeatability.

Declaration of competing interest

The authors declare that they have no known competing financial interests or personal relationships that could have appeared to influence the work reported in this paper.

Acknowledgment

S. A. Mozaffari acknowledges the support rendered by the Iranian Research Organization for Science and Technology (IROST) and Iran Nanotechnology Initiative Council (INIC).

References

Andrade, G., Barbosa-Stancioli, E. F., Mansur, A. P., Vasconcelos, W. L., & Mansur, H. S. (2006). Design of novel hybrid organic-inorganic nanostructured biomaterials for immunoassay applications. *Biomedical Materials, 1*(4), 221.

Ang, L. F., Por, L. Y., & Yam, M. F. (2013). Study on different molecular weights of chitosan as an immobilization matrix for a glucose biosensor. *PLoS One, 8*(8), Article e70597.

Ansari, S. G., Ansari, Z. A., Wahab, R., Kim, Y. S., Khang, G., & Shin, H. S. (2008). Glucose sensor based on Nano-baskets of tin oxide templated in porous alumina by plasma enhanced CVD. *Biosensors and Bioelectronics, 23*(12), 1838–1842.

Asrami, P. N., Azar, P. A., Tehrani, M. S., & Mozaffari, S. A. (2020). Glucose oxidase/nano-ZnO/thin film deposit FTO as an innovative clinical transducer: A sensitive glucose biosensor. *Frontiers in Chemistry, 8*, 503.

Asrami, P. N., Mozaffari, S. A., Tehrani, M. S., & Azar, P. A. (2018). A novel impedimetric glucose biosensor based on immobilized glucose oxidase on a CuO-chitosan nanobiocomposite modified FTO electrode. *International Journal of Biological Macromolecules, 118*, 649–660.

Asrami, P. N., Tehrani, M. S., Azar, P. A., & Mozaffari, S. A. (2017). Impedimetric glucose biosensor based on nanostructure nickel oxide transducer fabricated by reactive RF magnetron sputtering system. *Journal of Electroanalytical Chemistry, 801*, 258–266.

Bagyalakshmi, S., Sivakami, A., & Balamurugan, K. S. (2020). A Zno nanorods based enzymatic glucose biosensor by immobilization of glucose oxidase on a chitosan film. *Obesity Medicine*, 100229.

Barathi, P., Thirumalraj, B., Chen, S. M., & Angaiah, S. (2019). A simple and flexible enzymatic glucose biosensor using chitosan entrapped mesoporous carbon nanocomposite. *Microchemical Journal, 147*, 848–856.

Barman, A., De, A., & Das, M. (2019). Stabilization and dispersion of ZnO nanoparticles in PVA matrix. *Journal of Inorganic and Organometallic Polymers and Materials*, 1–10.

Branca, C., D'Angelo, G., Crupi, C., Khouzami, K., Rifici, S., Ruello, G., et al. (2016). Role of the OH and NH vibrational groups in polysaccharide-nanocomposite interactions: A FTIR-ATR study on chitosan and chitosan/clay films. *Polymer, 99*, 614–622.

Cánovas, R., Blondeau, P., & Andrade, F. J. (2020). Modulating the mixed potential for developing biosensors: Direct potentiometric determination of glucose in whole, undiluted blood. *Biosensors and Bioelectronics, 112302*.

Chen, R. H., Tsaih, M. L., & Lin, W. C. (1996). Effects of chain flexibility of chitosan molecules on the preparation, physical, and release characteristics of the prepared capsule. *Carbohydrate Polymers, 31*(3), 141–148.

Coates, J., & Meyers, R. A. (2000). Interpretation of infrared spectra, a practical approach. In *Encyclopedia of analytical chemistry* (pp. 10815–10837). Chichester: Wiley.

Dai, Z. H., Ni, J., Huang, X. H., Lu, G. F., & Bao, J. C. (2007). Direct electrochemistry of glucose oxidase immobilized on a hexagonal mesoporous silica-MCM-41 matrix. *Bioelectrochemistry, 70*(2), 250–256.

Dakshayini, B. S., Reddy, K. R., Mishra, A., Shetti, N. P., Malode, S. J., Basu, S., et al. (2019). Role of conducting polymer and metal oxide-based hybrids for applications in ampereometric sensors and biosensors. *Microchemical Journal, 147*, 7–24.

Dong, S., Zhang, J., Huang, G., Wei, W., & Huang, T. (2021). Conducting microporous organic polymer with-oh functional groups: Special structure and multi-functional integrated property for organophosphorus biosensor. *Chemical Engineering Journal*, 126682.

Duran, B. G., Castañeda, E., & Armijo, F. (2019). Development of an electrochemical impedimetric immunosensor for corticotropin releasing hormone (CRH) using half-antibody fragments as elements of biorecognition. *Biosensors and Bioelectronics, 131*, 171–177.

Dutta, P. K., Dutta, J., & Tripathi, V. S. (2004). Chitin and chitosan: Chemistry, properties and applications. *Journal of Scientific & Industrial Research, 63*, 20–31.

El-Naggar, M. E., & Shoueir, K. (2020). Recent advances in polymer/metal/metal oxide hybrid nanostructures for catalytic applications. *Journal of Environmental Chemical Engineering, 104175*.

Fadillah, G., Saputra, O. A., & Saleh, T. A. (2020). Trends in polymers functionalized nanostructures for analysis of environmental pollutants. *Trends in Environmental Analytical Chemistry, 26*, Article e00084.

Fatoni, A., Anggraeni, M. D., & Dwiasi, D. W. (2019). Easy and low-cost chitosan cryogel-based colorimetric biosensor for detection of glucose. *Journal of Analytical Chemistry, 74*(9), 933–939.

German, N., Ramanavicius, A., & Ramanaviciene, A. (2017). Amperometric glucose biosensor based on electrochemically deposited gold nanoparticles covered by polypyrrole. *Electroanalysis, 29*(5), 1267–1277.

Guan, H., Gong, D., Song, Y., Han, B., & Zhang, N. (2019). Biosensor composed of integrated glucose oxidase with liposome microreactors/chitosan nanocomposite for amperometric glucose sensing. *Colloids and Surfaces A: Physicochemical and Engineering Aspects, 574*, 260–267.

Gupta, S., Sharma, A., & Verma, R. S. (2020). Polymers in biosensor devices for cardiovascular applications. *Current Opinion in Biomedical Engineering, 13*, 69–75.

He, C., Liu, J., Zhang, Q., & Wu, C. (2012). A novel stable amperometric glucose biosensor based on the adsorption of glucose oxidase on poly (methyl methacrylate)–bovine serum albumin core–shell nanoparticles. *Sensors and Actuators B: Chemical, 166*, 802–808.

Kamyabi, M. A., Hajari, N., Turner, A. P., & Tiwari, A. (2013). A high-performance glucose biosensor using covalently immobilised glucose oxidase on a poly (2, 6-diaminopyridine)/carbon nanotube electrode. *Talanta, 116*, 801–808.
Kausaite-Minkstimiene, A., Glumbokaite, L., Ramanaviciene, A., & Ramanavicius, A. (2020). Reagent-less Amperometric glucose biosensor based on nanobiocomposite consisting of poly (1, 10-phenanthroline-5, 6-Dione), poly (Pyrrole-2-carboxylic acid), gold nanoparticles and glucose oxidase. *Microchemical Journal, 154*, 104665.
Kawahara, M., Yui, T., Oka, K., Zugenmaier, P., Suzuki, S., Kitamura, S., et al. (2003). Fourth 3D structure of the chitosan molecule: Conformation of chitosan in its salts with medical organic acids having a phenyl group. *Bioscience, Biotechnology, and Biochemistry, 67*(7), 1545–1550.
Kouhestanian, E., Mozaffari, S. A., Ranjbar, M., & Salar Amoli, H. (2020). Enhancing the electron transfer process of TiO2-based DSSC using DC magnetron sputtered ZnO as an efficient alternative for blocking layer. *Organic Electronics, 86*, 105915.
Kucherenko, I. S., Kucherenko, D. Y., Soldatkin, O. O., Lagarde, F., Dzyadevych, S. V., & Soldatkin, A. P. (2016). A novel conductometric biosensor based on hexokinase for determination of adenosine triphosphate. *Talanta, 150*, 469–475.
Kucherenko, I. S., Soldatkin, O. O., Kucherenko, D. Y., Soldatkina, O. V., & Dzyadevych, S. V. (2019). Advances in nanomaterial application in enzyme-based electrochemical biosensors: A review. *Nanoscale Advances, 1*(12), 4560–4577.
Kumar, R. V., Elgamiel, R., Koltypin, Y., Norwig, J., & Gedanken, A. (2003). Synthesis and characterization of a micro scale zinc oxide–PVA composite by ultrasound irradiation and the effect of composite on the crystal growth of zinc oxide. *Journal of Crystal Growth, 250*(3–4), 409–417.
Kumar, S., Nehra, M., Dilbaghi, N., Tankeshwar, K., & Kim, K. H. (2018). Recent advances and remaining challenges for polymeric nanocomposites in healthcare applications. *Progress in Polymer Science, 80*, 1–38.
Lertworasirikul, A., Tsue, S. I., Noguchi, K., Okuyama, K., & Ogawa, K. (2003). Two different molecular conformations found in chitosan type II salts. *Carbohydrate Research, 338*(11), 1229–1233.
Li, Y., Wang, N., Huang, X., Li, F., Davis, T. P., Qiao, R., et al. (2019). Polymer-assisted magnetic nanoparticle assemblies for biomedical applications. *ACS Applied Bio Materials, 3*(1), 121–142.
López-Chàvez, E., Solorza-Guzmàn, M., & de Landa Castillo-Alvarado, F. (2006). Advances in Science and Technology. In *Molecular simulation of ion-transport inside chitosan membranes* (pp. 188–198). Trans Tech Publ.
Macdonald, D. D. (1990). Some advantages and pitfalls of electrochemical impedance spectroscopy. *Corrosion, 46*(3), 229–242.
Macdonald, J. R., Schoonman, J., & Lehnen, A. P. (1982). Applicability and power of complex nonlinear least squares for the analysis of impedance and admittance data. *Journal of Electroanalytical Chemistry and Interfacial Electrochemistry, 131*, 77–95.
Mahadeva, S. K., & Kim, J. (2011). Conductometric glucose biosensor made with cellulose and tin oxide hybrid nanocomposite. *Sensors and Actuators B: Chemical, 157*(1), 177–182.
Mallakpour, S., & Madani, M. (2015). A review of current coupling agents for modification of metal oxide nanoparticles. *Progress in Organic Coatings, 86*, 194–207.
Marie, M., Mandal, S., & Manasreh, O. (2015). An electrochemical glucose sensor based on zinc oxide nanorods. *Sensors, 15*(8), 18714–18723.
Melo, A. F., Luz, R. A., Iost, R. M., Nantes, I. L., & Crespilho, F. N. (2013). Highly stable magnetite modified with chitosan, ferrocene and enzyme for application in magneto-switchable bioelectrocatalysis. *Journal of the Brazilian Chemical Society, 24*(2), 285–294.
Mohamed, S. A., Al-Harbi, M. H., Almulaiky, Y. Q., Ibrahim, I. H., & El-Shishtawy, R. M. (2017). Immobilization of horseradish peroxidase on Fe_3O_4 magnetic nanoparticles. *Electronic Journal of Biotechnology, 27*, 84–90.
Moharamzadeh, M., Salar Amoli, H., & Mozaffari, S. A. (2018). Fabrication of ultra-fast humidity ZITO nanoporous sensor by sol–gel technique for dynamic situation and human breath. *Journal of Sol-Gel Science and Technology, 85*(3), 596–609.
Mozaffari, S. A., Chang, T., & Park, S. M. (2009). Diffusional electrochemistry of cytochrome c on mixed captopril/3-mercapto-1-propanol self-assembled monolayer modified gold electrodes. *The Journal of Physical Chemistry C, 113*(28), 12434–12442.
Mozaffari, S. A., Chang, T., & Park, S. M. (2010). Self-assembled monolayer as a pre-concentrating receptor for selective serotonin sensing. *Biosensors and Bioelectronics, 26*(1), 74–79.
Mozaffari, S. A., Rahmanian, R., Abedi, M., & Salar Amoli, H. (2014). Urea impedimetric biosensor based on reactive RF magnetron sputtered zinc oxide nanoporous transducer. *Electrochimica Acta, 146*, 538–547.
Mozaffari, S. A., Salar Amoli, H., Simorgh, S., & Rahmanian, R. (2015). Impedimetric thiourea sensing in copper electrorefining Bath based on DC magnetron sputtered Nanosilver as highly uniform transducer. *Electrochimica Acta, 184*, 475–482.
Ocvirk, G., Buck, H., & DuVall, S. H. (2016). *Electrochemical glucose biosensors for diabetes care* (pp. 1–101). Trends in Bioelectroanalysis: Springer.
Ogawa, K., Yui, T., & Okuyama, K. (2004). Three D structures of chitosan. *International Journal of Biological Macromolecules, 34*(1–2), 1–8.
Okuyama, K., Noguchi, K., Kanenari, M., Egawa, T., Osawa, K., & Ogawa, K. (2000). Structural diversity of chitosan and its complexes. *Carbohydrate Polymers, 41*(3), 237–247.
Pastor-Fernández, C., Uddin, K., Chouchelamane, G. H., Widanage, W. D., & Marco, J. (2017). A comparison between electrochemical impedance spectroscopy and incremental capacity-differential voltage as Li-ion diagnostic techniques to identify and quantify the effects of degradation modes within battery management systems. *Journal of Power Sources, 360*, 301–318.
Pauporté, T. (2007). Highly transparent ZnO/polyvinyl alcohol hybrid films with controlled crystallographic orientation growth. *Crystal Growth and Design, 7*(11), 2310–2315.
Peng, Z., & Kong, L. X. (2007). A thermal degradation mechanism of polyvinyl alcohol/silica nanocomposites. *Polymer Degradation and Stability, 92*(6), 1061–1071.
Rahmanian, R., Mozaffari, S. A., & Abedi, M. (2015). Disposable urea biosensor based on nanoporous ZnO film fabricated from omissible polymeric substrate. *Materials Science and Engineering: C, 57*, 387–396.
Rassas, I., Braiek, M., Bonhomme, A., Bessueille, F., Rafin, G., Majdoub, H., et al. (2019). Voltammetric glucose biosensor based on glucose oxidase encapsulation in a chitosan-kappa-carrageenan polyelectrolyte complex. *Materials Science and Engineering: C, 95*, 152–159.
Sarkar, S., Guibal, E., Quignard, F., & SenGupta, A. K. (2012). Polymer-supported metals and metal oxide nanoparticles: Synthesis, characterization, and applications. *Journal of Nanoparticle Research, 14*(2), 715.
Sassolas, A., Blum, L. J., & Leca-Bouvier, B. D. (2012). Immobilization strategies to develop enzymatic biosensors. *Biotechnology Advances, 30*(3), 489–511.
Schué, F. (2000). In Z. Amjad (Ed.), *vol 49. Water soluble polymers: Solution properties and applications* (p. 417). New York: Plenum Press (4). 1998 Pp 259, ISBN 0-306-45931-0.
Shabani, R., Mozaffari, S. A., Husain, S. W., & Saber Tehrani, T. M. (2009). Selective nanosensing of copper (II) ion using L-lysine functionalized gold cysteamine self-assembled monolayer. *Iranian Journal of Science & Technology, Transaction A, 33*(A4), 335–347.
Shervedani, R. K., Bagherzadeh, M., & Mozaffari, S. A. (2006). Determination of dopamine in the presence of high concentration of ascorbic acid by using gold cysteamine self-assembled monolayers as a nanosensor. *Sensors and Actuators B: Chemical, 115*(2), 614–621.
Shervedani, R. K., & Mozaffari, S. A. (2006). Copper (II) Nanosensor based on a gold cysteamine self-assembled monolayer functionalized with salicylaldehyde. *Analytical Chemistry, 78*(14), 4957–4963.
Shukla, S. K., Deshpande, S. R., Shukla, S. K., & Tiwari, A. (2012). Fabrication of a tunable glucose biosensor based on zinc oxide/chitosan-graft-poly (vinyl alcohol) core-shell nanocomposite. *Talanta, 99*, 283–287.
Uwimbabazi, E., Mukasekuru, M. R., & Sun, X. (2017). Glucose biosensor based on a glassy carbon electrode modified with multi-walled carbon nanotubes-chitosan for the determination of beef freshness. *Food Analytical Methods, 10*(8), 2667–2676.
Wahab, R. A., Elias, N., Abdullah, F., & Ghoshal, S. K. (2020). On the taught new tricks of enzymes immobilization: An all-inclusive overview. *Reactive and Functional Polymers, 152*, 104613.
Wan, Y., Creber, K. A., Peppley, B., & Bui, V. T. (2003). Ionic conductivity of chitosan membranes. *Polymer, 44*(4), 1057–1065.
Wang, J. (2008). Electrochemical glucose biosensors. *Chemical Reviews, 108*(2), 814–825.
Wang, Q., Zhang, X., Huang, L., Zhang, Z., & Dong, S. (2017). GOx@ZIF-8 (NiPd) nanoflower: An artificial enzyme system for tandem catalysis. *Angewandte Chemie, 129*(50), 16298–16301.
Xu, L. C., Vadillo-Rodriguez, V., & Logan, B. E. (2005). Residence time, loading force, pH, and ionic strength affect adhesion forces between colloids and biopolymer-coated surfaces. *Langmuir, 21*(16), 7491–7500.
Xue, K., Zhou, S., Shi, H., Feng, X., Xin, H., & Song, W. (2014). A novel amperometric glucose biosensor based on ternary gold nanoparticles/polypyrrole/reduced graphene oxide nanocomposite. *Sensors and Actuators B: Chemical, 203*, 412–416.
Yang, K., She, G. W., Wang, H., Ou, X. M., Zhang, X. H., Lee, C. S., & Lee, S. T. (2009). ZnO nanotube arrays as biosensors for glucose. *The Journal of Physical Chemistry C, 113*(47), 20169–20172.
Yang, M., Yang, Y., Liu, B., Shen, G., & Yu, R. (2004). Amperometric glucose biosensor based on chitosan with improved selectivity and stability. *Sensors and Actuators B: Chemical, 101*(3), 269–276.
Yang, X., Shao, C., Guan, H., Li, X., & Gong, J. (2004). Preparation and characterization of ZnO nanofibers by using electrospun PVA/zinc acetate composite fiber as precursor. *Inorganic Chemistry Communications, 7*(2), 176–178.
Yang, Y. M., Wang, J. W., & Tan, R. X. (2004). Immobilization of glucose oxidase on chitosan–SiO_2 gel. *Enzyme and Microbial Technology, 34*(2), 126–131.
Zhang, W., Liu, C., Zou, X., Zhang, H., & Xu, X. (2020). Micrometer-scale light-addressable potentiometric sensor on an optical fiber for biological glucose determination. *Analytica Chimica Acta, 1123*, 36–43.